Hysteresis-free switching between vortex and collinear magnetic states

2014 New J. Phys. 16 053002

(http://iopscience.iop.org/1367-2630/16/5/053002)

New Journal of Physics
The open access journal at the forefront of physics
Deutsche Physikalische Gesellschaft DPG | IOP Institute of Physics

Hysteresis-free switching between vortex and collinear magnetic states

Erik Östman[1], Unnar B Arnalds[1], Emil Melander[1], Vassilios Kapaklis[1], Gunnar K Pálsson[2,3], Alexander Y Saw[2,3], Marc A Verschuuren[4], Florian Kronast[5], Evangelos Th Papaioannou[1], Charles S Fadley[2,3] and Björgvin Hjörvarsson[1]

[1] Department of Physics and Astronomy, Uppsala University, Box 516, SE-75120 Uppsala, Sweden
[2] Department of Physics, University of California at Davis, Davis, California 95016, USA
[3] Materials Sciences Division, Lawrence Berkeley National Laboratory, Berkeley, California 94720, USA
[4] Philips Research Laboratories, High Tech Campus 4, Eindhoven, The Netherlands
[5] Helmholtz Zentrum Berlin für Materialien und Energie, Albert-Einstein-Strasse 15, D-12489 Berlin, Germany
E-mail: erik.ostman@physics.uu.se

Received 13 December 2013, revised 7 March 2014
Accepted for publication 18 March 2014
Published 1 May 2014
New Journal of Physics **16** (2014) 053002
doi:10.1088/1367-2630/16/5/053002

Abstract

We demonstrate a lossless switching between vortex and collinear magnetic states in circular FePd disks arranged in a square lattice. Above a bifurcation temperature (T_e) we show that thermal fluctuations are enough to facilitate flipping between the two distinctly different magnetic states. We find that the temperature dependence of the vortex annihilation and nucleation fields can be described by a simple power law relating them to the saturation magnetization.

Keywords: magnetic nanostructures, magnetic vortices, thermal fluctuations

The experimental observation of the magnetic vortex state in circular islands [1] has attracted substantial interest within the field of nanomagnetism [2–9]. The range of envisioned applications is extensive, spanning from memory devices [10] to targeted cancer-cell destruction [11]. A magnetic vortex has four states defined by the polarity, the direction of

the out-of-plane moments, and the chirality, the direction of the curling of the in-plane moments. The bistable nature of the vortex polarity, pointing either up or down, has been the subject of intense study [12–15] and a bistability between the magnetic vortex and the collinear state has also been observed. Upon thermal annealing of individual cobalt islands grown on a ruthenium surface, Ding *et al* found that for certain sizes of the islands the magnetic state could be converted from a vortex state to a collinear state and vice versa [16]. Furthermore, thermally active nano-patterned magnetic materials have recently gained a lot of interest [17–21], where elongated islands fluctuate between two collinear states, different only in the direction of the magnetization. Here we investigate the effects of thermal fluctuations in arrays of thin circular disks. Our results provide a new perspective on the role of thermal excitations in magnetic nano systems, illustrated by the presence of a bistable region above a bifurcation temperature $\left(T_{\mathrm{e}}\right)$. Above this temperature, the thermal fluctuations are sufficient for transitions between the vortex state and the collinear state, leading to a hysteresis-free switching.

The magnetic field response of vortices is characterized by two critical fields, the annihilation field (H_{an}) and the nucleation field (H_{n}). Upon reaching H_{an}, the vortex is pushed out from the disk (i.e. annihilated), and the magnetization of the disk becomes close to collinear. A vortex reappears when the field is removed, albeit generally at a lower field H_{n}. This hysteresis between the annihilation and the nucleation fields can be viewed as arising from an energy barrier between the two states. A vortex state has a very low stray field and the interaction between even densely packed disks in the vortex state is therefore negligible. When an external field is applied, the vortex cores shift from the center of the disks, resulting in a net magnetization and a stray field. The energy landscape of vortices forming a dense array can therefore be tuned by the distance between the disks [3, 22–24] as well as through altering the inter-disk coupling by changing the disk material. Understanding the influence of interactions and temperature on the magnetic states is essential for obtaining a complete and consistent picture of the different magnetic phases and their boundaries. However, the use of materials having high intrinsic Curie temperatures (T_{C}) has severely limited the previously accessible range in magnetization [16, 25–27]. Using materials with experimentally accessible T_{C}, in which full magnetization is obtained at low temperatures and zero magnetization at and above the ordering temperature ($T \geqslant T_{\mathrm{C}}$), a maximum response is obtained. Here we utilize both the composition of the disks and the temperature to alter the energy landscape of the vortex/collinear state and thereby control the region of bistability.

Two samples with different FePd compositions, $Fe_{13.5}Pd_{86.5}$ and $Fe_{20}Pd_{80}$, were grown on $30 \times 30\ \mathrm{mm}^2$ pre-patterned fused silica substrates prepared by surface conformal nano-imprint lithography [28]. The samples were co-sputtered using elemental Fe(99.95 at-%) and Pd(99.95 at-%) targets in an ultra-high vacuum magnetron sputtering system with a base pressure below 2×10^{-7} Pa. Argon was used as the sputtering gas at a pressure of 0.8 Pa. The sample stage was rotated and the substrate kept at room temperature (RT) during growth. This resulted in highly uniform polycrystalline disks, see inset in figure 1(d). Each of the disks has a radius of $R = 225$ nm and a mean thickness of 10 nm. The lattice parameter of 513 nm gives an inter-disk distance $d = 63$ nm in the [10] direction and $d = 212.5$ nm in the [11] direction, well within the strong coupling regime of circular magnetic elements [22]. The saturation magnetization of 13.5 at-% and 20 at-% FePd compositions is $4.8 \times 10^5\ \mathrm{A\ m^{-1}}$ and $5.9 \times 10^5\ \mathrm{A\ m^{-1}}$ [29] with T_{C} ~300 K and ~500 K [30], respectively.

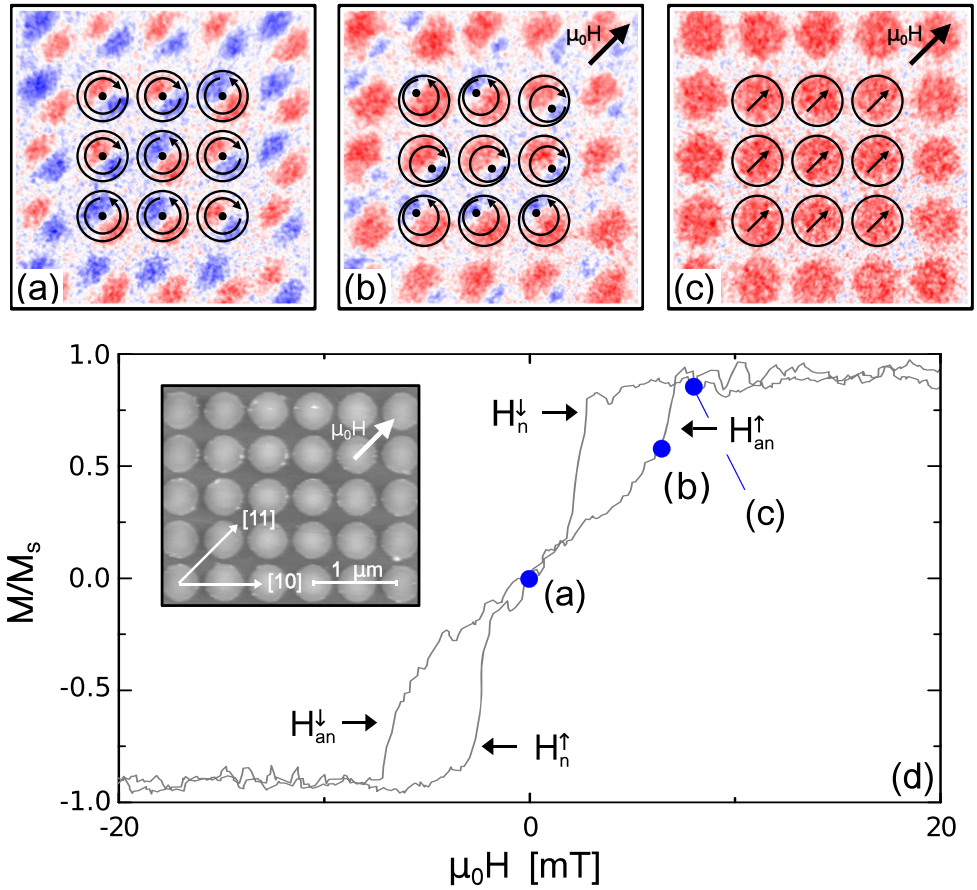

Figure 1. PEEM–XMCD images recorded at room temperature of the magnetic state in the disks for the $Fe_{20}Pd_{80}$ sample at (a) remanence, (b) close to the transition from a vortex state to a collinear state, and (c) under saturation, with a field applied in the [11] direction. Their respective positions on the magnetization loop are shown in (d). The inset shows an AFM image of the $Fe_{20}Pd_{80}$ sample defining the [10] and [11] directions.

Imaging of the field dependence of the magnetic vortex state was obtained using photoemission electron microscopy (PEEM), conducted at the elliptically polarized microfocus soft x-ray undulator beamline UE49-PGM-a-SPEEM at the BESSY-II synchrotron facility (Helmholtz Zentrum Berlin), which was equipped with the Elmitec PEEM-III endstation. Imaging was performed using low-energy secondary electrons with a probing depth of around 5 nm and a spatial resolution of 30 nm (field of view 5 μm). The Fe L_3 resonance (705.6 eV) was used to obtain magnetic contrast, with images taken using both right-hand and left-hand circularly polarized light (RCP and LCP). The magnetic contrast is obtained as the asymmetry ratio of intensities for LCP and RCP polarizations. The technique is sensitive to magnetic moments which have a component in the beam direction. Several series of nucleation and saturation events were recorded.

As a field is applied, the vortex cores move from the center of the disks towards the edges where they annihilate, as seen in figures 1(a), (b) and (c). The shift of the vortex center is perpendicular to the applied magnetic field and depends on the vortex chirality with respect to the direction of the applied field. The disks exhibited no evident memory of chirality upon field

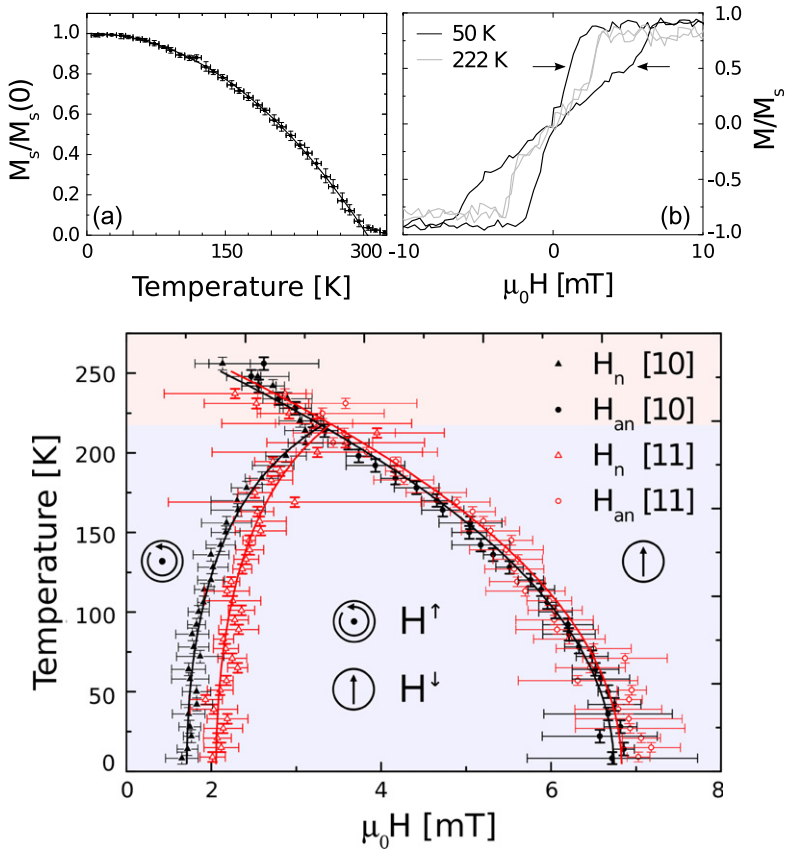

Figure 2. (a) Normalized magnetization in a field of 50 mT (black squares), and fit (solid line) using a modified Bloch behavior. (b) Normalized magnetization loops at two different temperatures, showing the presence and the absence of hysteresis in the magnetization loops. (c) Phase diagram for the $Fe_{13.5}Pd_{86.5}$ sample with H_n and H_{an} for the [10] and [11] directions defining the phase boundaries. The solid lines are fits made based on equation (1). Since two values of H_{an} and H_n exist in each loop, $H_{n(an)}$ is defined as $H_{n(an)} = \left(H^{\uparrow}_{n(an)} - H^{\downarrow}_{n(an)}\right)/2$, where the arrows indicate the direction of the applied field.

cycling. No general preferable chirality was seen, although clusters of up to 14 disks, and lines with up to ten disks in a row, with the same chirality, were observed.

The temperature dependence of the magnetization was investigated using the magneto-optical Kerr effect in a longitudinal configuration [31]. The incident laser beam (λ = 635 nm) had a spot size of $\sim$1 mm^2, averaging therefore the response of approximately four million disks. A magnetization loop at RT for the $Fe_{20}Pd_{80}$, with an external field applied in the [11] direction, is shown in figure 1(d). The results reveal a typical vortex behavior, with a sharp increase (decrease) of the magnetization at the field required for the vortex annihilation (nucleation). The individual magnetization loops for the $Fe_{13.5}Pd_{86.5}$ sample are comparable to the results obtained for the $Fe_{20}Pd_{80}$ sample on a reduced temperature scale. The magnetization as a function of temperature for the $Fe_{13.5}Pd_{86.5}$ sample, at a field of 50 mT, is displayed in figure 2(a). The solid line is a fit assuming a modified Bloch behavior:

$M(T) = M(0)\left(1 - \left(T/T_C\right)^{\alpha}\right)$ where T_C and α are fitting parameters. The fit yielded T_C = 307.9 ± 0.7 K, $\alpha = 2.11 \pm 0.02$ and $T_C = 462.5 \pm 2.3$ K and $\alpha = 1.69 \pm 0.02$ for the $Fe_{13.5}Pd_{86.5}$ sample and the $Fe_{20}Pd_{80}$ sample, respectively.

The field response of the magnetization obtained at 222 K differs significantly from what is observed at 50 K, as seen in figure 2(b). The nucleation and the annihilation fields are now the same and the switching between vortex and collinear states is hysteresis-free. The field dependence of the magnetization still displays typical vortex features, with a sharp increase (decrease) at annihilation (nucleation). The bifurcation temperature T_e at 212 K marks the onset of the collapse of the hysteresis, as illustrated in the phase diagram in figure 2(c). The temperature dependence of H_{an} and H_n for individual permalloy (Py) disks has previously been related to the decrease of M_s with increased temperature [25]. Thermal excitations within the islands influence H_{an} through oscillations of the vortex core [9]. Consequently, increased temperature will lead to larger oscillations, facilitating the annihilation process. For an array of disks the inter-disk interactions need to be included to obtain a more complete view of the creation–annihilation process.

In the absence of a full theoretical treatment of the effect of inter-disk coupling, we attempt the following phenomenological description of the relation between the critical fields and the magnetization.

$$H_{an(n)} \propto aM_s\left(T\right)^b \tag{1}$$

in which both a and b are fitting parameters. Instead of a linear response to M_s, an effective exponent, b, is introduced, capturing the effect of the inter-disk coupling. In this way we are able to relate both H_n and H_{an} to the intrinsic magnetic properties of the disks and the strength of the inter-disk coupling. H_n and H_{an} versus the reduced magnetization for the two samples are shown in figure 3. H_{an} decreases almost linearly with M_s with an exponent b close to one (see table 1) for the $Fe_{13.5}Pd_{86.5}$ sample, resembling results obtained from individual disks of Py [25]. Increasing the Fe content, figure 3(b), does not change the interrelation for H_{an} between the [10] and [11] directions, they are still indistinguishable. The absence of directional dependence of H_{an} does not by necessity imply non-existing inter-disk coupling in the annihilation process. Inter-disk coupling is known to stabilize the collinear state, decreasing both H_{an} and H_n [22–24]. The observed stabilization can thus be viewed as a bias field, increasing with decreasing distance between the disks and decreasing with increased temperature as the saturation magnetization (M_s) decreases. The shift of H_{an} is, however, intricate and involves the distribution of chirality of the vortex states since this will affect the stray field of each disk and that of its neighbors. The rigid vortex model [22] which has been successfully deployed earlier to describe various phenomena fails to explain this directional dependence. Supposedly the effective bias field, as the coupling can be described as, suppresses H_{an} equally in all directions. Even though no directional dependence is seen even for the Fe-rich sample, the exponent b decreases, see table 1, due to the increased inter-disk coupling, as expected from the increase in M_s.

The effect of the inter-disk coupling is more clearly seen for H_n which increases with decreasing M_s, the opposite to that of individual disks of Py [25]. Contrary to H_{an}, there is also a clear directional dependence for H_{an} arising from the different inter-disk distances in the [10]

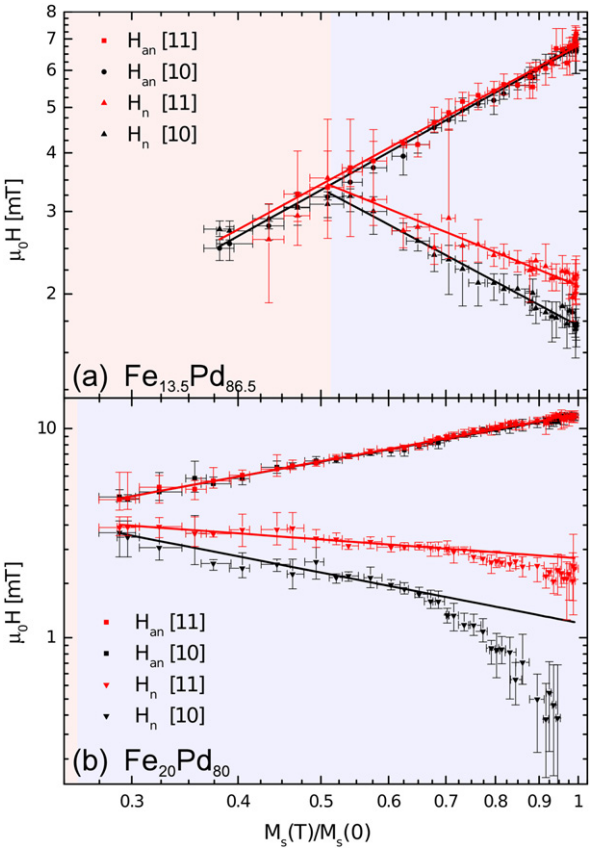

Figure 3. (a) Log–log plot of H_{an} and H_n versus normalized saturation magnetization in both the [10] and the [11] directions for the $Fe_{13.5}Pd_{86.5}$ sample. Solid lines are fits to equation (1). H_{an} is the same in both the [10] and the [11] directions whereas H_n shows a distinct difference between the two. Panel (b) shows the corresponding data for $Fe_{20}Pd_{80}$. The difference for H_n between the [10] direction and the [11] direction has increased due to a higher M_s and consequently higher inter-disk coupling. The higher $T_C = 462.5$ K shifts T_e to higher values. The graph is cut off at 0.2 on the horizontal axis for clarity. Above 0.7 M_s the hysteresis loops display a coercivity and the simple model, equation (1), is no longer applicable.

Table 1. Values of the exponent b in equation (1) for both samples obtained from the fits shown in figure 3.

		H_{an}	H_n
$Fe_{13.5}Pd_{86.5}$	[10]	1.06 ± 0.02	−0.97 ± 0.07
	[11]	0.99 ± 0.06	−0.74 ± 0.11
$Fe_{20}Pd_{80}$	[10]	0.74 ± 0.02	−0.80 ± 0.14
	[11]	0.76 ± 0.02	−0.30 ± 0.06

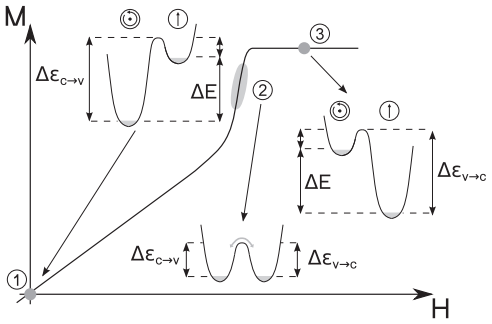

Figure 4. Schematic hysteresis loop above T_e together with the shifting energy landscape from (1) remanence to (3) saturation. In the transition region (2) the depth of the two energy minima, corresponding to the vortex and collinear states, are of the same order. At (1) k_BT is lower than the transition energy from a vortex to a collinear state $\Delta\varepsilon_{v\to c}$, while at (3) k_BT is lower than the transition energy from a collinear to a vortex state $\Delta\varepsilon_{c\to v}$.

and the [11] directions. The larger influence of inter-disk coupling in nucleation compared to annihilation can be understood considering the collinear state and the larger effective bias field strength relative to the applied field, since the nucleation occurs at much lower fields. Increasing the Fe content results in an increased M_s and thus increased stray field, which in turn means an increased coupling leading to an enhanced splitting in the directional dependence of H_n. Increasing the temperature decreases the directional difference as a result of the reduced inter-disk coupling. The larger inter-disk coupling for the Fe-rich sample is also reflected in the b values where the difference for b in the [10] and the [11] directions is significantly increased.

The energy landscape of the array above T_e in the bistable region is schematically depicted in figure 4. In the absence of an external field (marked (1) in the figure), the energy of the vortex state is lower than the collinear state. The opposite is valid at (3), at which the collinear state has lower energy. The energy difference between the two states (ΔE) will therefore have to approach zero at some field strength, giving rise to a bistable condition. In the transition region marked as (2), ΔE is small and the transition between the two different states will be dictated by the activation barrier. Here we have to distinguish between two extreme cases: one where the transition energy barrier $\Delta\varepsilon \gg k_BT$ and one where $\Delta\varepsilon \ll k_BT$. When both $\Delta\varepsilon_{v\to c}$ and $\Delta\varepsilon_{c\to v}$ (the energy barriers for transitions from vortex to collinear states and vice versa) are larger than k_BT, the bi-stability will give rise to hysteresis, characteristic for the vortex annihilation and nucleation. However, when $\Delta\varepsilon_{v\to c}$ and $\Delta\varepsilon_{c\to v}$ are smaller than k_BT, the switching will occur without hysteresis, as illustrated in figure 4 and seen in figure 2(c).

To conclude, a bistable region with hysteresis-free transition between collinear and vortex states is obtained when $T > T_e$. Below T_e, the switching between the vortex and the collinear states exhibit hysteresis and the transition is irreversible. Above T_e, thermally induced bistability is obtained ($T_c > T > T_e$). In this bistable region, thermal fluctuations alone are enough for switching between the vortex and the collinear state. These findings enable the exploration of dynamics in a wider temperature range and provide a new insight into and pathways for the study of bistability in magnetic nano systems, such as artificial spin ice systems [21]. The hysteresis-free switching of vortices is not only of academic interest, it also has significant

implications for applications of magnetic nano structures in spintronic devices, discrete recording media or magnetic field sensors [32, 33].

Acknowledgments

The authors acknowledge the support of the Knut and Alice Wallenberg Foundation, the Swedish Research Council, and the Swedish Foundation for International Cooperation in Research and Higher Education.

References

[1] Shinjo T, Okuno T, Hassdorf R, Shigeto K and Ono T 2000 Magnetic vortex core observation in circular dots of permalloy *Science* **289** 930–2
[2] Cowburn R P, Koltsov D K, Adeyeye A O, Welland M E and Tricker D M 1999 Single-domain circular nanomagnets *Phys. Rev. Lett.* **83** 1042–5
[3] Novosad V, Guslienko K Yu, Shima H, Otani Y, Kim S G, Fukamichi K, Kikuchi N, Kitakami O and Shimada Y 2002 Effect of interdot magnetostatic interaction on magnetization reversal in circular dot arrays *Phys. Rev.* B **65** 060402
[4] Metlov K L and YoungPak L 2008 Map of metastable states for thin circular magnetic nanocylinders *Appl. Phys. Lett.* **92** 112506
[5] Chung S-H, McMichael R D, Pierce D T and Unguris J 2010 Phase diagram of magnetic nanodisks measured by scanning electron microscopy with polarization analysis *Phys. Rev.* B **81** 024410
[6] Zhang W, Singh R, Bray-Ali N and Haas S 2008 Scaling analysis and application: phase diagram of magnetic nanorings and elliptical nanoparticles *Phys. Rev.* B **77** 144428
[7] Guslienko K Yu 1999 Magnetostatic interdot coupling in two-dimensional magnetic dot arrays *Appl. Phys. Lett.* **75** 394–6
[8] Zarzuela R, Vélez S, Hernandez J M, Tejada J and Novosad V 2012 Quantum depinning of the magnetic vortex core in micron-size permalloy disks *Phys. Rev.* B **85** 180401
[9] Machado T S, Rappoport T G and Sampaio L C 2012 Vortex core magnetization dynamics induced by thermal excitation *Appl. Phys. Lett.* **100** 112404
[10] Bohlens S, Kruger B, Drews A, Bolte M, Meier G and Pfannkuche D 2008 Current controlled random-access memory based on magnetic vortex handedness *Appl. Phys. Lett.* **93** 142508
[11] Kim D-H, Rozhkova E A, Ulasov I V, Bader S D, Rajh T, Lesniak M S and Novosad V 2010 Biofunctionalized magnetic-vortex microdiscs for targeted cancer-cell destruction *Nat. Mater.* **9** 165–71
[12] deLoubens G *et al* 2009 Bistability of vortex core dynamics in a single perpendicularly magnetized nanodisk *Phys. Rev. Lett.* **102** 177602
[13] Van Waeyenberge B *et al* 2006 Magnetic vortex core reversal by excitation with short bursts of an alternating field *Nature* **444** 461–4
[14] Guslienko K Yu, Lee K-S and Kim S-K 2008 Dynamic origin of vortex core switching in soft magnetic nanodots *Phys. Rev. Lett.* **100** 027203
[15] Curcic M *et al* 2008 Polarization selective magnetic vortex dynamics and core reversal in rotating magnetic fields *Phys. Rev. Lett.* **101** 197204
[16] Ding H F, Schmid A K, Dongqi L, Guslienko K Y and Bader S D 2005 Magnetic bistability of co nanodots *Phys. Rev. Lett.* **94** 157202
[17] Arnalds U B, Farhan A, Chopdekar R V, Kapaklis V, Balan A, Papaioannou E Th, Ahlberg M, Nolting F, Heyderman J L and Hjörvarssou B 2012 Thermalized ground state of artificial kagome spin ice building blocks *Appl. Phys. Lett.* **101** 112404

[18] Kapaklis V *et al* 2012 Melting artificial spin ice *New J. Phys.* **14** 035009
[19] Farhan A, Derlet P M, Kleibert A, Balan A, Chopdekar R V, Wyss M, Perron J, Scholl A, Nolting F and Heyderman L J 2013 Direct observation of thermal relaxation in artificial spin ice *Phys. Rev. Lett.* **111** 057204
[20] Zhang S, Gilbert I, Nisoli C, Chern G-W, Erickson M J, OBrien L, Leighton C, Lammert P E, Crespi V H and Schiffer P 2013 Crystallites of magnetic charges in artificial spin ice *Nature* **500** 553–7
[21] Farhan A, Derlet P M and Kleibert A 2013 Exploring hyper-cubic energy landscapes in thermally active finite artificial spin-ice systems *Nat. Phys.* **9** 375–82
[22] Guslienko K Yu, Novosad V, Otani Y, Shima H and Fukamichi K 2001 Magnetization reversal due to vortex nucleation displacement and annihilation in submicron ferromagnetic dot arrays *Phys. Rev.* B **65** 024414
[23] Chao C-T, Kuo C-Y, Tsai Y-C, Chang C K, Wang J F, Horng L and Jong-Ching W 2011 Study of inter-dot coupling in nano-patterned permalloy dots array *JPCS* **266** 012005
[24] Gubbiotti G, Madami M, Tacchi S, Socino G, Carlotti G and Okuno T 2006 Effect of interdot dipolar coupling on the magnetic properties of permalloy nano-cylinders *Surf. Sci.* **600** 4143–6
[25] Mihajlovic G, Patrick M S, Pearson J E, Novosad V, Bader S D, Field M, Sullivan G J and Hoffmann A 2010 Temperature dependent nucleation and annihilation of individual magnetic vortices *Appl. Phys. Lett.* **96** 112501
[26] Streubel R, Makarov D, Kronast F, Kravchuk V, Albrecht M and Schmidt O G 2012 Magnetic vortices on closely packed spherically curved surfaces *Phys. Rev.* B **85** 174429
[27] Burgess J A J, Fortin D C, Losby J E, Grombacher D, Davis J P and Freeman M R 2010 Thermally activated decay of magnetic vortices *Phys. Rev.* B **82** 144403
[28] Pierret A, Hocevar M, Diedenhofen S L, Algra R E, Vlieg E, Timmering E C, Verschuuren M A, Immink G W G, Verheijen M A and Bakkers E P A M 2010 Generic nano-imprint process for fabrication of nanowire arrays *Nanotechnology* **21** 065305
[29] Zhang S L, Sumiyama K and Nakamura Y 1988 Magnetic properties of nonequilibrium bcc and fcc Fe-Pd alloys produced by vapor quenching *J. Magn. Magn. Mater.* **73** 58–64
[30] Büscher C, Auerswald T, Scheer E, Schröder A, Löhneysen H v and Claus H 1992 Ferromagnetic transition in dilute Fe-Pd alloys *Phys. Rev.* B **46** 983–9
[31] Papaioannou E T, Kapaklis V, Taroni A, Marcellini M and Hjörvarsson B 2010 *J. Phys.: Condens. Matter* **22** 236004
[32] Novosad V, Fradin F Y, Roy P E, Buchanan K S, Yu K, Guslienko and Bader S D 2005 Magnetic vortex resonance in patterned ferromagnetic dots *Phys. Rev.* B **72** 024455
[33] Bader S D 2006 Colloquium: opportunities in nanomagnetism *Rev. Mod. Phys.* **78** 1–15